Global Change Biology

Global Change Biology (2011) **17**, 2245–2260, doi: 10.1111/j.1365-2486.2011.02405.x

Relationships between phenology, radiation and precipitation in the Amazon region

ANDREW V. BRADLEY*, FRANCE F. GERARD†, NICOLAS BARBIER‡, GRAHAM P. WEEDON§, LIANA O. ANDERSON¶‖, CHRIS HUNTINGFORD†, LUIZ E. O. C. ARAGÃO**, PRZEMYSLAW ZELAZOWSKI¶ and EGIDIO ARAI‖

*Department of Geography, University of Leicester, Leicester LE1 7RH, UK, †Centre for Ecology and Hydrology, Wallingford, Oxfordshire OX10 8BB, UK, ‡IRD-UMR AMAP, Boulevard de la Lironde, TA A-51/PS2, 34398 Montpellier, Cedex 05, France, §Hadley Centre for Climate Prediction and Research, Met. Office, Joint Centre for Hydrometeorological Research, Wallingford, Oxfordshire OX10 8BB, UK, ¶Environmental Change Institute, Oxford University Centre for the Environment, Oxford OX13QY, UK, ‖Remote Sensing Division, National Institute for Space Research – INPE, Avenida dos Astronautas, 1.758-Jd. Granja-CEP 12227-010, Brazil, **College of Life and Environmental Sciences, University of Exeter, Exeter EX4 4RJ, UK*

Abstract

In tropical areas, Dynamic Global Vegetation Models (DGVMs) still have deficiencies in simulating the timing of vegetation phenology. To start addressing this problem, standard Fourier-based methods are applied to aerosol screened monthly remotely sensed phenology time series (Enhanced Vegetation Index, EVI) and two major driving factors of phenology: solar radiation and precipitation (for March 2000 through December 2006 over northern South America). At 1×1 km scale, using power (or variance) spectra on good quality aerosol screened time series, annual cycles in EVI are detected across 58.24% of the study area, the strongest (largest amplitude) occurring in the savanna. Terra Firme forest have weak but significant annual cycles in comparison with savannas because of the heterogeneity of vegetation and nonsynchronous phenological events within 1×1 km scale pixels. Significant annual cycles for radiation and precipitation account for 86% and 90% of the region, respectively, with different spatial patterns to phenology. Cross-spectral analysis was used to compare separately radiation with phenology/EVI, precipitation with phenology/EVI and radiation with precipitation. Overall the majority of the Terra Firme forest appears to have radiation as the driver of phenology (either radiation is in phase or leading phenology/EVI at the annual scale). These results are in agreement with previous research, although in *Acre*, central and eastern Peru and northern Bolivia there is a coexistence of 'in phase' precipitation over Terra Firme forest. In contrast in most areas of savanna precipitation appears to be a driver and savanna areas experiencing an inverse (antiphase) relationship between radiation and phenology is consistent with inhibited grassland growth due to soil moisture limitation. The resulting maps provide a better spatial understanding of phenology–driver relationships offering a bench mark to parameterize ecological models.

Keywords: Amazonia, cross-spectral analysis, Fourier, MODIS EVI, phenology, savanna, seasonality, Terra Firme forest, time series, vegetation modelling

Received 19 August 2010; revised version received 7 January 2011 and accepted 14 January 2011

Introduction

The Amazon region covers a significant area of the global landmass and predictions indicate land-cover or climatic change in this area could have regional and global impacts on the Earth system (Houghton *et al*., 2001; Silva Dias *et al*., 2002; Werth & Avissar, 2002; Asner *et al*., 2004; Salazar *et al*., 2007). Computer models also predict, with some uncertainty, that climate change may involve feedbacks that alter atmospheric CO_2 concentrations such as dieback in north-east Amazonia contributing to increased CO_2 emissions from soil carbon stocks (Cox *et al*., 2000, 2004). A key factor in modelling the biosphere–atmosphere interface is being able to simulate vegetation activity, i.e. cycles of dormancy, active growth and reproduction, referred to as the phenology cycle. The correct representation of tropical phenology in vegetation models remains a research challenge particularly as most algorithms have been developed with an understanding of temperate climates e.g. the land surface model of the Joint UK Land Environment Simulator (JULES, Best, 2005). To improve Dynamic Global Vegetation Models (DGVMs) a better understanding of spatial and seasonal variation in phenology is needed. We begin to address this challenge by exploring where, which and to what extent climate factors, specifically solar

Correspondence: Andrew V. Bradley, tel. + 44 116 252 3823, fax + 44 116 252 3854, e-mail: avb4@le.ac.uk

radiation and precipitation, drive phenology in the Amazonian tropics.

Around the Amazon region much of the knowledge of annual vegetation activity has been gained from point specific *in situ* measurements. Seasonal cycles of vegetation activity have been calculated from flux tower measurements in Brazil, where differences in wet and dry ecosystem fluxes of CO_2 and H_2O have been calculated (Miranda *et al*., 1997; Malhi *et al*., 1998; Vourlitis *et al*., 2001, 2004). There have been direct observations of seasonal vegetation activity from phenology events like leaf and flower production across various tropical forests (Wright & van Schaik, 1994); flowering and fruiting observations at the Urucu river central Amazonia (Peres, 1994); flowering, leaf flushing and abscission in Purús, Amazonia (Haugaasen & Peres, 2005) and litter fall collections across the Amazon (Chave *et al*., 2010). In the surrounding savanna regions, measurements of litter fall have also been made in the Brazilian Cerrado (Valenti *et al*., 2008) and phenology observations have been made in the Venezuelan savanna (Monasterio & Sarmiento, 1976). There have also been synoptic observations of vegetation seasonality using satellite data. These include measuring the amplitude of MODIS Leaf Area Index (LAI) for the whole Amazon (Myneni *et al*., 2007); using time series profiles of AVHRR Normalized Difference Vegetation Index (NDVI) and Soil Adjusted Vegetation Index (SAVI) (Ferreira *et al*., 2003); recording signatures of Cerrado and forested areas in Brazil at high spectral resolution (Ferreira & Huete, 2004); and estimating forest deciduousness from spectral mixture analysis and NDVI of Landsat images in Panama (Bohlman, 2010).

In the Amazon region, with the exception of places at high altitude, temperature is generally considered as being high enough to not limit the seasonal growth of vegetation (Nemani *et al*., 2003). On the ground, research shows that, when precipitation has a strong seasonality, the phenology cycle is constrained during the dry season (Reich & Borchert, 1984) but also that phenology events can be a response to peaks in solar irradiance (Wright & van Schaik, 1994). Satellite evidence shows that in the Amazon basin changes in LAI do not necessarily follow precipitation gradients and the timing of net leaf flushing can be driven by the seasonality of solar radiation (Myneni *et al*., 2007). In Brazil increases in vegetation greening, measured with the Enhanced Vegetation Index (EVI), correspond to radiation increases and seasonally low precipitation (Huete *et al*., 2006) and if the forest canopy has a low density, productivity can be correlated with plant available water and vapour pressure deficit (Brando *et al*., 2010).

The role of soil moisture in phenology cycles is complex due to the spatial heterogeneity in the characteristics of soils and soil profiles (Quesada *et al*., 2009) and the variation in the soil water reserve due to interannual variability of different meteorological conditions, including drought (Phillips *et al*., 2009). Soil moisture has been shown to have widely different influences at individual research sites in Brazil: at the Reserva Biológica do Cuierias, central Amazonia, photosynthesis appears to be controlled by a lack of soil moisture in the dry season (Malhi *et al*., 1998) while in Pará State, eastern Amazonia, evapotranspiration of trees can continue in the dry season because deep rooting vegetation can penetrate down to available soil water (Nepstad *et al*., 1994; da Rocha *et al*., 2004). The advantage of deep roots has also been demonstrated across several sites in Northern Brazil where during the dry season forests with deep roots green up while pasture with shallow roots do not (Huete *et al*., 2006). Localized environmental conditions can also control phenology by influencing local plant physiology and adaptation. Malhado *et al*., (2009) found that the occurrence of small leaves may be related to water availability. Fyllas *et al*. (2009) discovered that the presence of certain leaf nutrients may have a positive relationship with precipitation and a weak relationship to soil.

On longer time scales, interannual variation of constraining factors can influence vegetation activity. Drought events have been linked to variations in vegetation greenness (Saleska *et al*., 2007; Oliveira *et al*., 2010; Samanta *et al*., 2010, 2011) and death of some trees (Nepstad *et al*., 2007). When Amazonian rain forests were exposed to a longer and more intense moisture deficit than normal, increases in mortality and decreases in growth induced losses in biomass (Phillips *et al*., 2009) and from 2000 through 2009 net primary productivity fell (Zhao & Running, 2010). On the other hand, cloud cover can cause interannual and decadal variations in tropical radiation budgets (Wielicki *et al*., 2002). The results of Nemani *et al*. (2003) showed that reduced cloud cover and increased tropical radiation from 1982 through 1999 contributed to $\sim$2% of the increase in global net primary productivity. If phenology–driver relations remain poorly understood, these variations could have significant impacts on the estimates of global fluxes and emissions.

Despite the spatial and temporal variations of controls between individual study sites, specific environmental conditions can be linked to phenology cycles. Haugaasen & Peres (2005) could divide the phenology events of an area according to whether their study locations were Terra Firme or seasonally flooded forest and from the analysis of sites on the regional scale correlations have been made between leaf litter seasonality and rainfall seasonality (Chave *et al*., 2010). These findings show that it should be possible to summarize phenology controls according to the composition of

Amazon forest which can occur in pockets (Coronado *et al*., 2009), as old-growth, flooded and seasonal forest (Chave *et al*., 2010) and evergreen and deciduous patches (Bohlman, 2010).

Several approaches have been applied to identify large scale variations in (leaf) phenology and its relationship to potential drivers on the basis of Earth Observation (EO) time series. For example, (i) comparing precipitation data to understand the onset of greenness and land cover variation in the Great Basin, United States (Bradley & Mustard, 2005; Bradley *et al*., 2007); (ii) to explore how different precipitation conditions influenced plant phenology in Etosha National Park, Namibia (Wagenseil & Samimi, 2006); (iii) to investigate how landscape variables of soil and land cover type influenced landscape variability in the Southern Great Plains, United States (Jakubauskas *et al*., 2002) and; (iv) vegetation–driver relationships have been investigated to understand the relationships of precipitation, radiation and vegetation globally (Nemani *et al*., 2003; Zhao & Running, 2010) and in South America (Huete *et al*., 2006; Myneni *et al*., 2007; Saleska *et al*., 2007; Samanta *et al*., 2010, 2011).

Evidence suggests that Amazon vegetation may be water limited (Zhao & Running, 2010) or conversely dominated by solar irradiance, reinforced by greening up during the 2005 drought (Huete *et al*., 2006; Saleska *et al*., 2007). The extent and cause of greening has been strongly contested with the revised and aerosol screened MODIS collection 5 (c5) product. The results of Saleska *et al*. (2007) are unrepeatable, there are no links to solar irradiance and nonpersistent anomalous greening can occur anywhere in any year (Samanta *et al*., 2010, 2011). Furthermore, ground-based measurements of increased tree mortality collected in 2005 do not support greening (Phillips *et al*., 2009). Alternative mechanisms that cause EVI increases during drought have been put forward: leaf flushing and bud development becomes synchronized (Brando *et al*., 2010); there are structural changes in the canopy after leaf loss (Anderson *et al*., 2010) and leaf loss in the tallest trees reduces the shade fraction (Anderson *et al*., 2011).

In the largely inaccessible Amazon region, there is still a lack of clarity for ecosystem modellers in the timing of phenology events, the strength in seasonality of phenology cycles and a spatial summary of the influence and timing of the phenology driving forces. Here we apply Fourier analysis to EO derived time series of vegetation indices, radiation and precipitation to identify where and when radiation and precipitation interact with annual leaf phenology cycles. The overall approach is to study average patterns observed in the time series, as opposed to anomalous years or long-term trends, to highlight the main phenology–driver relationships. The specific aims are to: (i) map the spatial heterogeneity of phenology cycles by calculating the intensity in seasonality of the leaf phenology cycle and (ii) map the spatial extent and timing of annual phenology–driver relationships. We describe the most commonly observed relationships in more detail and discuss how our results concur with the idea that radiation drives Terra Firme rainforest. The outcome of this research is a spatial benchmark of phenology drivers to assist in the modelling of leaf phenology in DGVMs.

Study area

We concentrated on the northern half of the South American continent, Fig. 1, which includes a wide range of vegetation types (Eva *et al*., 2004) and ecoregions (Olson *et al*., 2001). Terra Firme humid forest makes up the central area and this tends to be surrounded by seasonal forest and savanna to the north, east and south. Patches of flooded forest also exists in these areas. To the west are the montane forests of the Andes which grade into shrub and grasslands. Much of the west coast is desert which we do not consider. The study area extends beyond the Amazon basin covered by the map of Myneni *et al*. (2007) (the map shows the distribution of seasonal amplitudes of LAI), enabling us to show the contrast between Terra Firme, savanna and grassland regions while providing a more detailed perspective to the global map of Nemani *et al*. (2003) (the map shows the global geographic distribution of potential climatic constraints to plant growth).

The humid forests are classified Koeppen Af-Am tropical wet climates. Annual rainfall can exceed 2000–3000 mm, with up to three months below 100 mm (Sarmiento & Monasterio, 1975), for gradients see Fig. 1, of Malhado *et al*. (2009). The savanna regions, with the exception of isolated areas in the humid forest belt, are classified as Koeppen Aw tropical wet and dry climates. Annual rainfall totals are around 1000–2000 mm yr^{-1}, with a wet season of 5–8 months (Sarmiento & Monasterio, 1975). In typical dry forest, e.g. Cerrado, annual rainfall ranges from 1000 to 2000 mm. In montane forests, totals can be 800–2500 mm depending on the altitude. Totals for grass and shrubland may range from 400 to 1500 mm (Bradley & Millington, 2006).

Materials

The three EO time series analysed are EVI (phenology), solar radiation and precipitation covering almost 7 years. The overlap of the time series was constrained from the first available year of phenology data (2000) through to the last available year of the radiation data (2006).

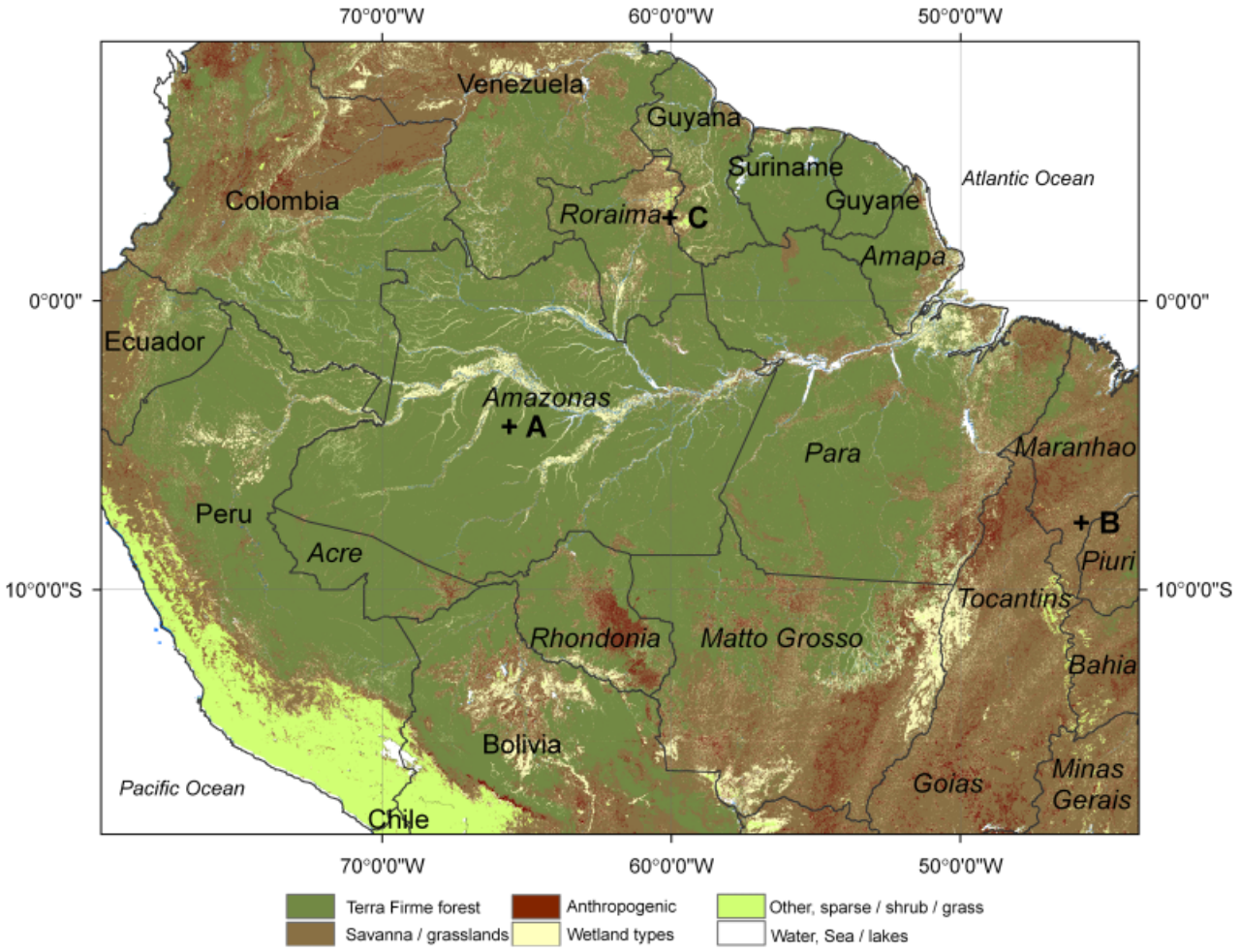

Fig. 1 The study area covers approximately $10.4 \times 10^6\,km^2$ between latitudes of 9.0°N and 18.5°S and longitudes 43.8°W and 79.8°W. The main vegetation types are shown and are derived from subclasses of Saatchi *et al*. (2007) (subclasses in brackets): Terra Firme forest (dense forest, open forest, bamboo forest, Liana/dry forest, seasonal forest); Savanna and grassland type (dense woodland, open woodland, park/shrubland, grassland); Wetland type (closed forest, open forest, herbaceous, mangrove); Anthropogenic type (secondary/degraded forest, nonforest pasture, crops/bare). Countries are marked except for Brazil where states are labelled in italics. Location A, B and C are approximate locations of time series examples referred to in the text.

EVI

For the leaf phenology, we used the product MOD13A3 c5 of the Moderate Resolution Imaging Spectroradiometer (MODIS). This product provides, among other parameters and spectral bands, monthly composites of the EVI at 1×1 km resolution (Huete *et al*., 2002). The EVI is calculated from the blue, red and near-infrared channels:

$$\mathrm{EVI} = \frac{G \times (\rho\mathrm{NIR} - \rho\mathrm{red})}{(\rho\mathrm{NIR} + C1 \times \rho\mathrm{red} - C2 \times \rho\mathrm{blue} + L)}, \qquad (1)$$

where red is the centre frequency of 6.45 μm; NIR the near-infrared centre frequency of 8.65 μm; ρ the reflectance, G the gain factor 2.5 and $C1$ and $C2$ are the coefficients of aerosol resistances 6 and 7.5, respectively; and L the canopy background adjustment 1.0.

EVI is considered to be closely related to canopy structure, type and architecture and has been shown to give improved sensitivity than other vegetation indices, e.g. NDVI, in high biomass regions, such as tropical forests (Huete *et al*., 2002) by decoupling the canopy background signal and reducing atmospheric influences. This VI is also considered to be appropriate for the savanna regions since Ferreira & Huete (2004) found SAVI, an index conceptually similar to EVI, dealt with canopy shadow effects better than NDVI in the Brazilian Cerrado.

The c5 product was downloaded from the NASA LP DAAC archive. To cover the study area, we needed 12 tiles (1200 lines $\times$ 1200 columns): H10v08–H13v08; H10v09–H13v09; and H10v10–H13v10. These tiles were processed using the MODIS Reprojection Tool (MRT, 2008) to create monthly mosaics then stacked chronologically to produce phenology time series from March 2000 to December 2006. Using a monthly time series reduces the impact of anomalous pixels by selecting the

maximum EVI value between the daily images of the same month (Huete *et al*., 1999), for more detail see Anderson *et al*. (2010). Additional screening of the data was made by eliminating pixels marked with the MODIS QA flags for clouds, shadow, climatology, medium and high aerosols similar to the procedures of Samanta *et al*. (2010, 2011).

Radiation

The time series of downward (incoming) shortwave radiation are modelled estimates from the *Centro de Previsão de Tempo de Estudos Climaticos* (CPTEC) GL-1.2 physical model (Ceballos *et al*., 2004). The GL-1 model uses hourly measurements from the GOES-8 geostationary satellite and estimates the radiation budget in three broadband widths in the UV (μm not specified), visible (0.4–0.7 μm) and near-infrared (0.7–3.0 μm). The final radiation budget is calculated at several heights from the Earth's surface at a resolution of $0.4 \times 0.4^{\circ}$. We used monthly averages of the daily surface irradiation for the time period 2000–2006. The advantage of this data set is that the hourly frequency of observations account for daily cloud development. A disadvantage is that surface reflectance, a function of the vegetation, is a component of the radiation calculation which may put a small bias on the vegetation–radiation relationships.

Precipitation

Precipitation time series from 2000 to 2006 inclusive were sourced from the product 3B43v6, named as, 'TRMM data and other sources precipitation data set' (NASA, 2006) derived mainly from satellite data acquired from TRMM (Kummerow *et al*., 1998). Monthly estimates at $0.25 \times 0.25^{\circ}$ resolution were downloaded from the Goddard Distributed Active Archive Centre. These data are based on average rates of precipitation in $\mathrm{mm\,h^{-1}}$.

Vegetation map

We used the vegetation map of South America, downloaded from the Distributed Active Archive Center (DAAC), (see Saatchi *et al*., 2007 p821 and http://www-radar.jpl.nasa.gov/carbon/ab/lclu_metadata.htm, last accessed July 2010) created from a hierarchical decision tree based on biomass levels and seasonality using fused optical (SPOT VEGETATION) and microwave (GRFM JERS-1) remote sensing data. We merged the classes into the following groups (Fig. 1): 'Terra Firme forest' classes (1–7, forest types); 'savanna and grassland' classes (8 and 10, wood and grassland); 'wetland' classes (11–15, various forest and grasslands) and 'other types' which included anthropogenic classes (16 and 17), high altitude shrub and grasslands (class 18).

Methods

The Fourier transform

The Fourier transform (FT), is a well established and efficient methodology to analyse time series data (Jenkins & Watts, 1968; Bloomfield, 1976; Priestley, 1981; Diggle, 1989; Weedon, 2003) and can be used for the detection of regular cycles, even when hidden in a noisy background. The extraction of information from the output of the FT has previously been used on satellite data to: classify land cover (Jakubauskas *et al*., 2001; Moody & Johnson, 2001); clean image time series (Lunetta *et al*., 2006; Hermance, 2007); track interannual variability of phenology for different land cover classes (Jakubauskas *et al*., 2002; Wagenseil & Samimi, 2006; Hermance *et al*., 2007); and characterize textural patterns of Terra Firme forest in the spatial domain (Barbier *et al*., 2010). The FT can be used to estimate a power spectrum that indicates the average variance in a time series at different time scales or frequencies. Standard linear detrending of the data before application of the FT allows an analysis of a 'stationary' time series as the mean and variance should ideally be more-or-less constant. At the frequency of the annual cycle, the power spectra can be used to identify the presence, absence and significance of a peak and this can be used as a measure of the strength (amplitude) of the annual cycle. Spectral peaks that exceed the 90% confidence level above the lag-1 autoregressive spectral background model (AR1 or 'red noise' of Mann & Lees, 1996, e.g. see Weedon, 2003) are termed significant peaks here. The power spectra were rescaled into relative power (i.e. the power at each frequency divided by the power at all frequencies). This rescaling has the advantage of allowing comparison of spectral results between variables with very different absolute ranges (e.g. EVI vs. radiation).

Cross-spectral analysis: coherency and phase

Cross-spectral analysis of remotely sensed time series has been successfully demonstrated by Aragão *et al*. (2008), comparing precipitation, fire counts and deforestation. Here we compare phenology with radiation and precipitation. For locations where there is an annual cycle in both the phenology time series and a driver, cross-spectral analysis, is used to simultaneously estimate the coherency (i.e. degree of correlation at specific frequencies; range: 0.0–1.0) and timing difference (termed phase difference or often simply 'phase'). Phase spectra can be used to establish the average relative timing or phase value ('lead' or 'lag') of the two variables at specific frequencies. Phase values also have a phase error and the 95% confidence interval of the phase error is related in a nonlinear fashion to the coherency (Bloomfield, 1976). At the annual scale phase can range from -6 to $+6$ months. The weaker the coherency, the larger the phase error and the more uncertain the phase value is (Fig. 4.16 of Weedon, 2003). Phase and phase error can be recorded in degrees or radians ($180^{\circ} = 2\pi$ radians) and can then be converted to the same time units as the original data. We express our results in months, therefore at the annual scale a phase difference of 90° is equivalent to $(90/360) \times 12$ months $= 3$ months. The key to identifying cycles which are significantly different from noise is to have a time series of observations which is at least five times longer than the period of the cycle of interest given a data interval (or sampling rate) of the time series that is small enough to avoid aliasing (Weedon, 2003).

Categorizing phase

The phase relationships were grouped into four categories, 'in phase', 'antiphase', 'leads' and 'lags'. The categorization used

a range or 'tolerance' for identifying 'in-phase' relationship ($0 \pm 30^\circ$ or 0.0 ± 1.0 months) or 'antiphase' relationship ($\pm 180 \pm 30^\circ$ or $\pm 6.0 \pm 1.0$ months). If the phase error (95% confidence) of a value was statistically indistinguishable from these classes, i.e. inside these ranges, then it was assigned as 'in phase' or 'antiphase', otherwise the value became 'lead' or 'lag'. The four categories are:

1. *driver and the phenology are 'in phase'*: The phase value is statistically indistinguishable (given the phase error) from $0 \pm 30^\circ$ (or 0.0 ± 1.0 months);
2. *driver 'leads' the phenology*: A positive phase that is between $+30^\circ$ (or $+1.0$ month) and $+150^\circ$ (or $+5.0$ months);
3. *driver and the phenology are 'in antiphase'*: A phase value that is statistically indistinguishable from $\pm 180 \pm 30^\circ$ (or $\pm 6.0 \pm 1.0$ months);
4. *driver 'lags' the phenology*: A negative phase between -30° (or -1.0 months) and -150° (or -5.0 months).

We checked the robustness of this categorization for the ± 1 month tolerance for the 'in-phase' and 'antiphase' categories by tightening and relaxing the tolerance to ± 0.5 months ($\pm 15^\circ$) and ± 1.5 months ($\pm 45^\circ$). This method is a robust statistical classification of phenology-driver phase differences avoiding manual thresholds which were dependent on the data set (Bradley *et al*., 2009).

Data processing

The processing involved four steps. First, the EVI data was prepared for (i) the investigation into the seasonality of the 1×1 km phenology time series, time series with more than 40% of screened points were termed 'incomplete' and ignored [grey areas of Fig. 2a(i)]; and (ii) for the cross-spectral analysis, to avoid a bias towards the presence of larger phenology amplitudes all remaining 1×1 km EVI/phenology points were averaged, to the resolution of the precipitation (0.25°) and radiation (0.4°) data. Secondly, standard linear detrending was carried out on all time series and using the FT, we determined for each pixel (i.e. image grid cell) the presence or absence of significant annual cyclical behaviour (i.e. seasonality) in the phenology (at 1×1 km, $0.4 \times 0.4^\circ$ and $0.25 \times 0.25^\circ$, Fig. 2a), radiation ($0.4 \times 0.4^\circ$, Fig. 2b) and precipitation ($0.25 \times 0.25^\circ$, Fig. 2c) time series and recorded the strength in seasonality. Thirdly, where significant annual cycles occurred, the cross-spectral analysis was used to compare pairs of time series to give a measure of coherency and phase differences. Finally, the phase value and phase error were used to categorize the phase relationships between radiation and phenology, between precipitation and phenology and between precipitation and radiation. These relationships were then mapped (Fig. 3).

Mapping phase categories and vegetation types

The phase-relationship categories, one for phenology–radiation and one for phenology–precipitation were mapped and overlain with the modified Saatchi *et al*. (2007) vegetation map of the Amazon region. The proportion of each phase relationship category in each vegetation type was calculated to determine the proportions of each phase relationship in each vegetation class. This allowed us to re-examine the theory of a dominantly radiation driven Amazon (Huete *et al*., 2006; Myneni *et al*., 2007).

Results

Strength of annual cycle – power spectrum

A large proportion of the Amazon and surrounding area shows significant annual cycles in radiation, precipitation and phenology (Fig. 2a–c). These results are reasonable since annual cycles, or seasonality, have been observed at research sites across the Amazon through a combination of precipitation, radiation and leaf litter fall measurements, in tropical rainforest, (Malhi *et al*., 1998; Huete *et al*., 2006), transitional tropical forest (Vourlitis *et al*., 2001, 2004) and savanna (Miranda *et al*., 1997). Figure 2a(i–iii) shows the distribution of the strength of the phenology cycle across our study area represented by the relative power for the annual cycle of the EVI. Screening out incomplete time series in the 1×1 km phenology analysis left 66.42% (6.9×10^6 km^2) of clean time series, 58.28% (6.1×10^6 km^2) reach at least the 90% confidence level in power, while 8.14% (0.8×10^6 km^2) show no significant or detectable annual cycle. Aerosol contamination is most acute in the Atlantic countries and *Para* in the north-east of the study area.

Areas where the annual phenology cycle are the strongest (i.e. good time series, significant and high relative power of at least 0.15) are located to the north in central Venezuela (the Orinoco Llanos), south and south-eastern states of Brazil (the Cerrado) and in southern parts of Bolivia and Peru (mainly the Bolivian llanos), and cover $\sim$66% or 1.9×10^6 km^2 of the savanna and grassland class area. This is consistent with ground observations of seasonality in savanna vegetation: Ferreira *et al*. (2003) found distinct wet and dry season spectral signatures and vegetation indices for Cerrado grass and woodland in Brasilia National Park, 16°30′00″S; 47°75′00″W; Valenti *et al*. (2008) observed synchronized leaf litter fall from woody plants during dry periods in São Paulo state, 21°58′12″S; 47°52′01″W; and; Sarmiento & Monasterio (1975) noted a strong seasonality in the phenology of the vegetation in many of the different savanna types of South America.

Areas where the annual phenology cycle tends to be weak (i.e. good time series, significant but low relative power <0.15) cover $\sim$49% or 2.6×10^6 km^2 of the Terra Firme forest class with the weakest power found in the northern areas of Brazil and Peru and the southern areas of Venezuela and Colombia. Approximately, 39% (2.11×10^6 km^2) of the area defined as Terra Firme forest have incomplete time series at 1×1 km resolution.

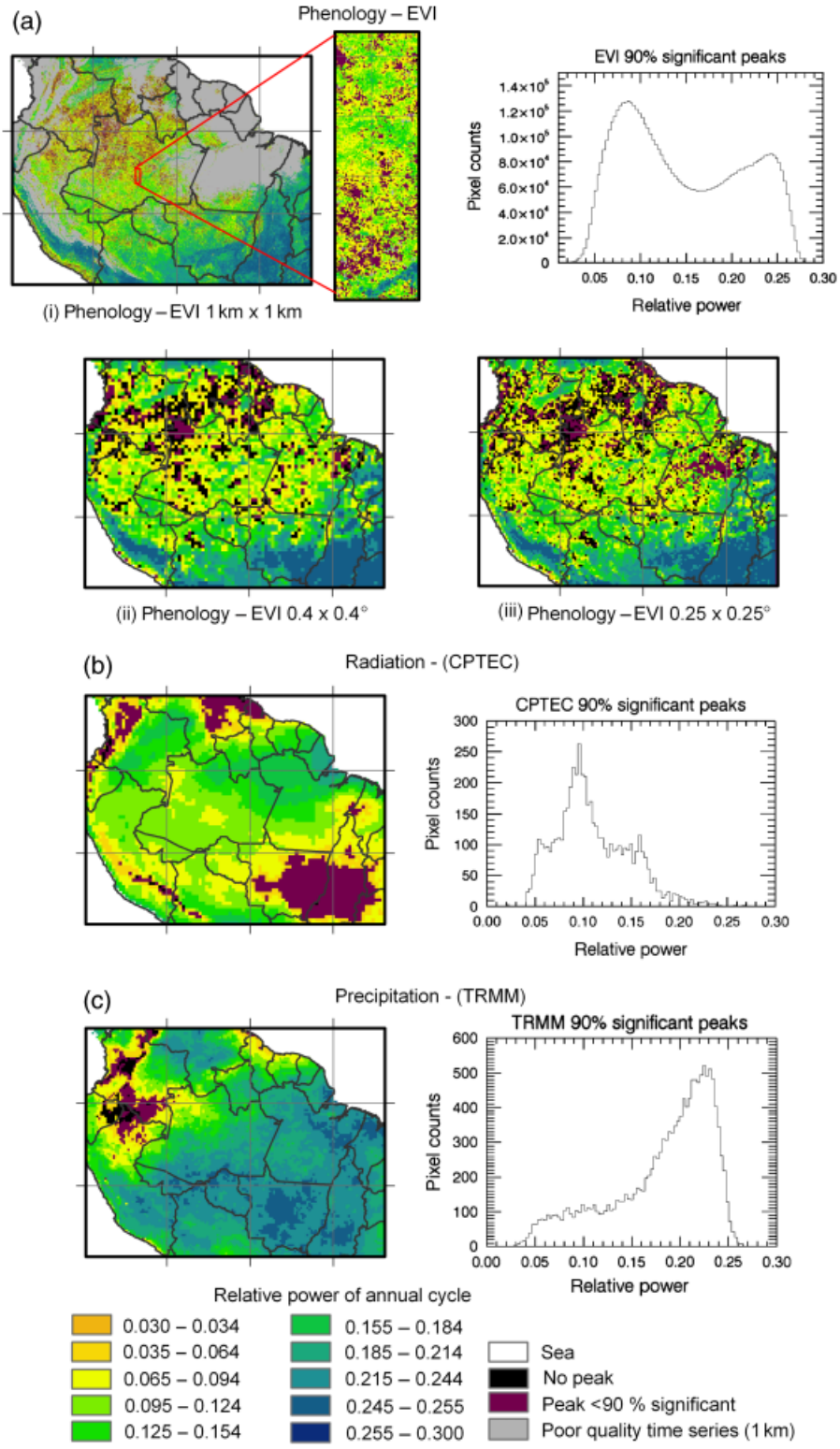

Fig. 2 (a–c) Spatial distribution and frequency distribution of relative power of the annual cycle for: (a) Phenology-EVI, (i) 1×1 km with bad time series screen (ii) $0.4 \times 0.4^{\circ}$ and (iii) $0.25 \times 0.25^{\circ}$; (b) Radiation-CPTEC; and (c) Precipitation-TRMM. Pixels that have spectral peaks that fell below the 90% significance threshold for background noise but still have annual peaks are shown in maroon; areas in black have no spectral peak at the annual scale.

Allowing for resolution differences, the time series aggregation, at the $0.4 \times 0.4^{\circ}$ and $0.25 \times 0.25^{\circ}$ scales, compensated for large areas of data rejection in the north-east in the primary 1×1 km EVI data. We have confidence in the strength of seasonality in the aggregated EVI maps where time series were excluded as incomplete, because Fig. 2a(ii and iii) generally replicate the patterns in the analysed areas of Fig. 2a(i). In the north-east, seasonality is moderate to low (0.03–0.18) and weak or no seasonality occurs in patches mainly in the Atlantic countries and Brazilian states Amazonas Roraima and Pará.

With respect to radiation, 86% of the land area has annual cycles above the 90% confidence level (Fig. 2b). The annual cycles are the strongest (i.e. highest power values) in Colombia and northern Brazil, Pará, Roraima and Amazonas, and gradually decrease to weak annual cycles in south central Brazil, Mato Grosso and Goiás, to the edge of the landmass between Ecuador and Guyana, and straddling the Peru–Bolivia border on the north-east flank of the Andes Mountains. Less than 1% of the area has no peak at all and this is found scattered across the Andean mountains.

For precipitation, the annual cycles above the 90% confidence level cover 95% of the land area (Fig. 2c). Most of the region shows a strong annual cycle with the exception of areas covering northern Peru, Ecuador and parts of Colombia, where annual cycles are $<90\%$ significant or have no peak at all. There is also an area of weaker but significant annual cycles over the Atlantic coast countries.

Comparing pairs of time series – cross-spectral analysis

Figure 3 shows the results of the radiation-EVI (Fig. 3a–c), precipitation-EVI (Fig. 3d–f) cross-spectral analysis using ± 0.5, ± 1.0 and ± 1.5 month tolerances. All categories, in phase, lags, leads and in antiphase, were represented. These categories of phase relationship vary between and within vegetation classes informing us that the timing between annual phenology cycles and each driver is variable across the whole Amazon and not necessarily specific to a particular vegetation type. Where neither driver is coherent with EVI at the annual scale, or where both drivers lag EVI/phenology other regional and localized drivers, than local solar radiation or precipitation, should be sought (see 'Discussion').

The grey areas of Fig. 3 show where at least one time series had no significant annual peak and/or where coherency is below the 95% confidence level (0.695). Using the ± 1.0 month tolerance, the areas of 'incomplete' time series and nonsignificant peaks for the phenology–radiation was 26.39% (2.74×10^6 km^2) with an additional 4.43% (0.46×10^6 km^2) of noncoherent pairs mainly in the south-east and north of the study area (Fig. 3b). For phenology–precipitation, the areas of bad time series and nonsignificant peaks was 22.77% (2.35×10^6 km^2) with an additional 6.45% (0.67×10^6 km^2) of noncoherent pairs, mainly in the north, north-west and the east of the study area (Fig. 3e).

The phase between precipitation and radiation (Fig. 3h) is roughly divided across Amazonas state, which is in antiphase in the north and east, and precipitation lags radiation in the south and west. Within these areas precipitation leads radiation in Guyana, Suriname and parts of Colombia and Venezuela and there is a small area where precipitation is in phase with radiation in the south. The driver phase classes are not specific to a single land cover type. Where the drivers are in antiphase, single driver relationships with phenology are strongest.

Figure 4a–h show the percentage of phase distribution values for each phase category (using the ± 1 month tolerance used in the rest of the paper) for each variable–phenology (EVI) pair. The phase error criteria divided the data into more-or-less unimodal phase difference categories. There is a slight lead of approximately 1 month of each driver over phenology in the in-phase category suggesting that there is always a slight lag period when phenology responds to a driver, we cannot reduce this as our time step is 1 month. The tolerance range of ± 1 month is wide enough to accommodate the slight lead and not pose a problem for the phase difference classification and our interpretations.

Phase relationships and vegetation types

The statistics for the spatial distribution of the phase difference categories in relation to vegetation are shown in Tables 1 and 2. In the case of radiation–phenology (Fig. 3b, Table 1), 16.8% of the area ($\sim 1.75 \times 10^6$ km^2), falls into the in-phase category-1 of which 72.6% represents Terra Firme forest and 11.9% savanna and grassland cover types. The leads category-2 makes up 38.1% ($\sim 3.96 \times 10^6$ km^2) of which 62.0% is Terra Firme forest and 18.8% is savanna and grassland. The remaining phase categories cover a small percentage of the area. Overall, there is a widespread in-phase or leading relationship between radiation and phenology mainly associated with Terra Firme forest. When considering precipitation–phenology (Fig. 3e, Table 2), 39.4% of the area ($\sim 4.11 \times 10^6$ km^2) falls into the 'in-phase' category-1 of which 38.0% is savanna and grassland and 37.7% is Terra Firme forest. 21.6% of the area ($\sim 2.26 \times 10^6$ km^2) corresponded to the lags category-4 of which 80.5% is Terra Firme forest. All the other phase categories cover small percentages of the area apart from 36.7% of the leads category which coincides with the shrub and grasslands land cover in the Andean Mountains. Overall, there is a widespread in-phase relationship between precipitation and phenology which is largely associated with savanna and grassland

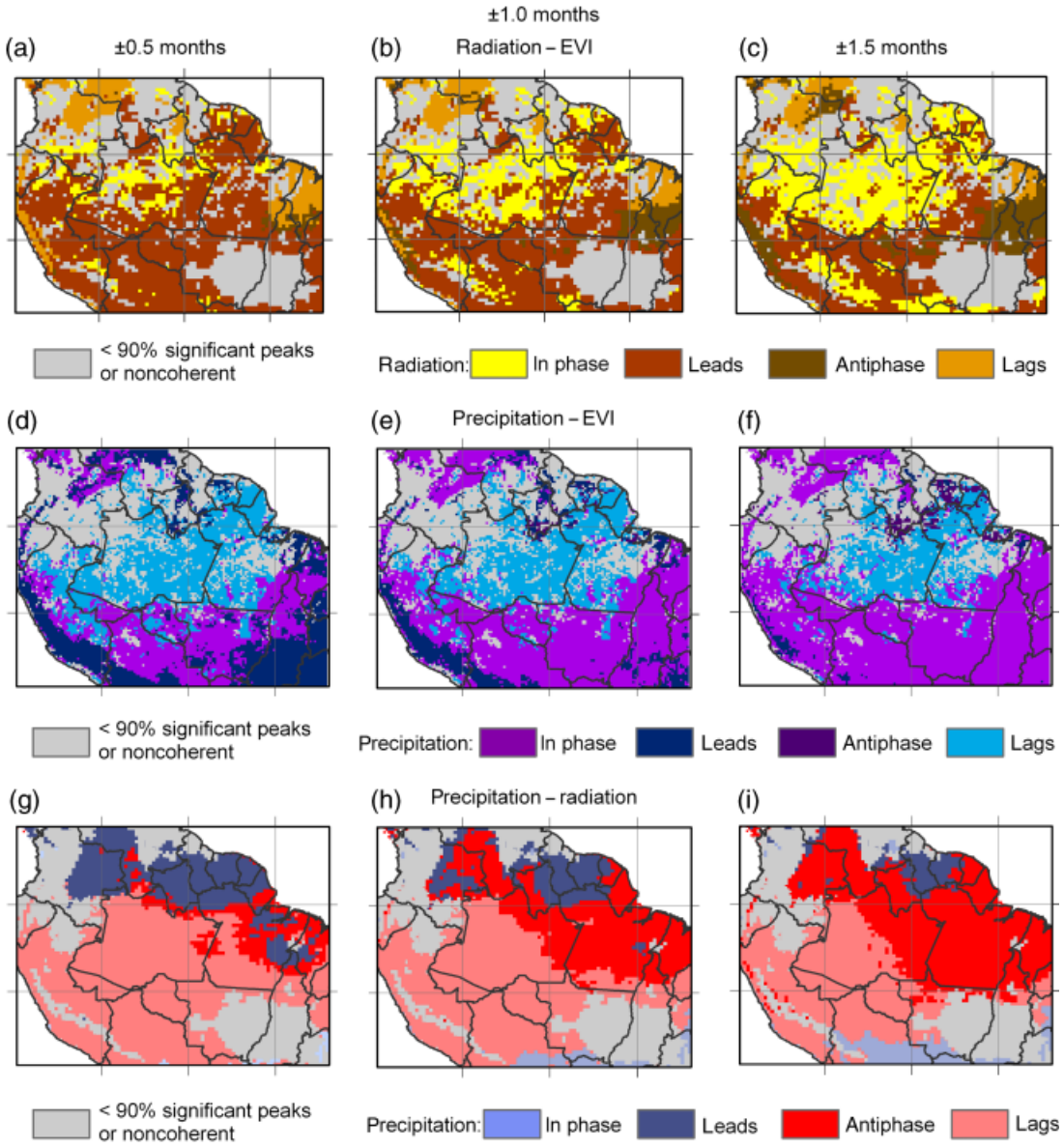

Fig. 3 (a–f) Phenology-driver phase categories at the annual scale in northern South America given ± 0.5, ± 1.0 and ± 1.5 month phase error tolerances. Using: (a–c) Radiation-EVI; (d–f) Precipitation-EVI; and (g–i) Precipitation-radiation.

and Terra Firme forest cover types. Where precipitation lags or is in antiphase with phenology large proportions of the area, 80.5% and 60.7%, respectively, are made up of Terra Firme forest.

Combined radiation and precipitation phase differences

To the south-east of the Amazon basin in Fig. 5, there is a large region where there is no significant annual cycle in the radiation data (i.e. no significant spectral peak, Fig. 2b). Consequently, it is not meaningful to use the cross-spectral results with the other variables at the annual scale in this region. Similarly, to the north-west of the Amazon basin there are large patches where the EVI and/or precipitation data do not show annual cycles (Fig. 2a and c). Nevertheless, in the great majority of the area studied, significant annual cycles in EVI coincide spatially with annual cycles in precipitation and/or radiation. In this section, we consider the phase categories in areas where both of the drivers, radiation and precipitation, are coherent with EVI/phenology (i.e. the coloured areas of Fig. 5a and b).

Where at least one of the drivers is in phase with phenology (Fig. 5a) vegetation is responding to the

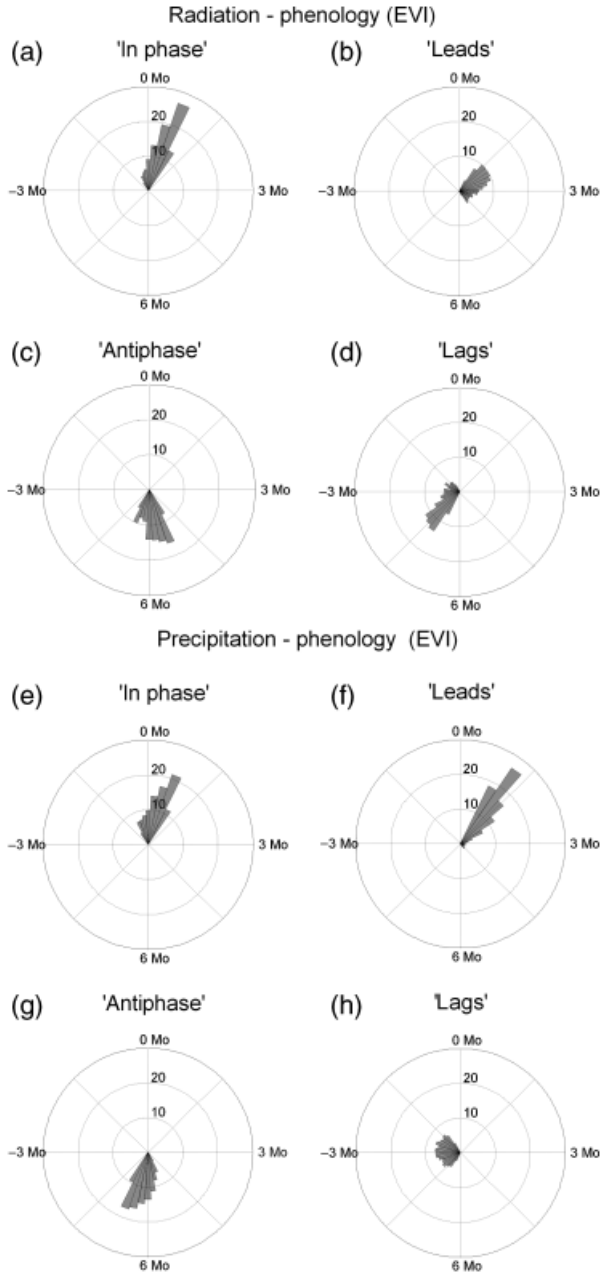

Fig. 4 (a–h): Phase difference characteristics for ± 1.0 month within each of the four classes, 'in phase', 'leads', 'antiphase' and 'lags' for radiation-phenology (a–d) and precipitation-phenology (e–h). The concentric rings are percentages, and the scale on the outer circle is the phase value in months.

driver(s) within a month. Radiation in phase with phenology (classes 4 and 5) mainly covers the Amazon basin and corresponds to the Terra Firme forest. In class 5, the fact that precipitation lags or is in antiphase with phenology while radiation is in phase, indicates that in these regions phenology is probably radiation, but certainly not precipitation driven. In class 4, radiation is in phase, but precipitation leads phenology. In such locations, the vegetation may respond to variations in leading precipitation (i.e. occurring between 2 and 5 months), perhaps replenishing soil moisture deficits, as well as to variations in solar radiation (e.g. inversely to cloud cover) within the current month.

Precipitation is in phase with phenology (classes 1 and 2) to the south and central north of the study region; this is mainly in savanna locations (Fig. 5a). In class 1 areas of Fig. 5a radiation lags or is in antiphase with phenology suggesting that the variation in precipitation is driving the phenology. Of particular note is a part of class 2 that occurs over Terra Firme forest in the south-west of the Amazon basin where precipitation is in phase with phenology and radiation leads phenology. This roughly corresponds with seasonal forests and confirms that not all the Terra Firme forest is solely radiation driven. If we consider an area in the south-east of the study area where there are no annual cycles in radiation (Fig. 2b), shown as light grey in Fig. 5a which mainly coincides with the hilly-mountainous area around Brasilia, precipitation is coherent and in phase with and apparently controlling the phenology (Fig. 3d–f). Statistically in-phase radiation and phenology as well as precipitation and phenology (class 3) only coincide in small patches to the north, the west and south-west of the whole study area; in most of the Amazon region only one driver is in phase with phenology.

Figure 5b shows where neither climate driver is in phase with the phenology indicating places where significant delays between the drivers and vegetation responses occur. Phenology may have a delayed response to precipitation to the west and south-west (classes 6 and 7) and a delayed response to radiation in the central areas (classes 6 and 8). Some of the areas coloured in Fig. 5b correspond to areas of anthropogenic disturbance, drainage networks and mountain regions where other drivers may be dominating phenology cycles.

To illustrate examples of the phase difference patterns in Fig. 5, time series at three sites A, B and C, are shown (Fig. 6 location on Fig. 1). Table 3 contains the relative annual power, coherency and phase values calculated for the time series (phenology, precipitation and radiation) of the three sites using the ± 1 month tolerance. These examples have been chosen for clarity, as in many cases the periodicity in the time series is concealed in a noisy signal where weak yet significant periodic cycles are still detected by the FT.

Location A (Fig. 6a) is situated in Terra Firme forest. Here both phenology and radiation have significant but weak annual cycles (i.e. low relative power values that are above the 90% confidence level). There is high coherency between phenology and radiation (0.83) and the two variables are statistically 'in phase' at the

Table 1 Location, area and land cover statistics for phenology–radiation ± 1.0-month phase tolerance categories

Phase: (category) and class	Approximate location	Area (10^6 km^2)	Area (%)	Terra Firme (%)	Savanna (%)	Wetland (%)	Other (%)
(1) In	Central Bolivia, south-east and north-east Peru, east Ecuador, southern Colombia, Suriname, *Amazonas*, *Roraima* and the west of *Para* state.	1.75	16.8	72.6	11.9	9.1	6.4
(2) Leads	Bolivia, south and central Peru, Brazilian states to the south and east of *Amazonas* excluding *Maranhão* and *Tocantins*.	3.96	38.1	62.0	18.8	5.5	13.7
(3) Anti	Mainly in Brazil, *Maranhão*, *Piauí*, *Tocantins* and north and western parts of the study area.	0.54	5.2	13.5	54.0	7.7	24.8
(4) Lags	Parts of east Colombia, western Venezuela, *Roraima* and *Piauí* states.	0.85	8.2	11.8	51.0	9.0	28.2
< 90% confidence in peaks or noncoherent	Mainly in Colombia, Venezuela, Ecuador, *Matto Grosso*, *Goiás* and scattered through Peru, Boliva, *Amazonas* and *Para states*.	3.30	31.7	46.0	29.8	10.3	13.9

Total land area at 0.4° = ~10.40×10^6 km^2.

Table 2 Location, area and land cover statistics for phenology–precipitation ± 1.0-month phase tolerance categories

Phase: (category) and class	Location	Area (10^6 km^2)	Area (%)	Terra Firme (%)	Savanna (%)	Wetland (%)	Other (%)
(1) In	Bolivia, central Peru, northern Colombia, south Venezuela, and Brazilian states to the south and east of *Amazonas* and *Para*.	4.11	39.4	37.7	38.0	9.3	15.0
(2) Leads	Mainly confined to the Atlantic countries and *states* to the north-east, *states* to the south-west of the study area and along the Andes mountains to the west.	0.92	8.8	16.3	27.5	8.3	47.9*
(3) Anti	Mainly confined to Suriname, Guyane, and Brazilian states *Roraimia* and north-west *Para*.	0.10	1.0	60.7	11.1	14.1	14.1
(4) Lags	East Peru, south Venezuela, Guyane, Brazilian states *Amazonas*, *Para*, and *Amapa*.	2.26	21.6	80.5	8.1	6.1	5.3
< 90% confidence in peaks or noncoherent	Mainly in north Peru, Ecuador, Colombia, east Venezuela, Guyana, north-east *Amazonas* and central *Para*.	3.06	29.2	59.8	21.7	7.1	11.4

Total land area at 0.25° = ~10.45×10^6 km^2.
*36.7% in shrub and grasslands.

annual scale (+ 0.13 ± 0.63 months, Table 3). Precipitation also has a strong annual cycle and coherency with phenology above the 95% significance threshold (0.79) but lags phenology (−4.13 ± 0.88 months). In this particular case, the phenology cannot be driven by precipitation given the lagging relationship, but is in phase with radiation. Location B (Fig. 6b) is positioned in the savanna and grassland class. Both phenology and precipitation show strong annual cycles (relative power above 0.24). The two variables have a significant coher-

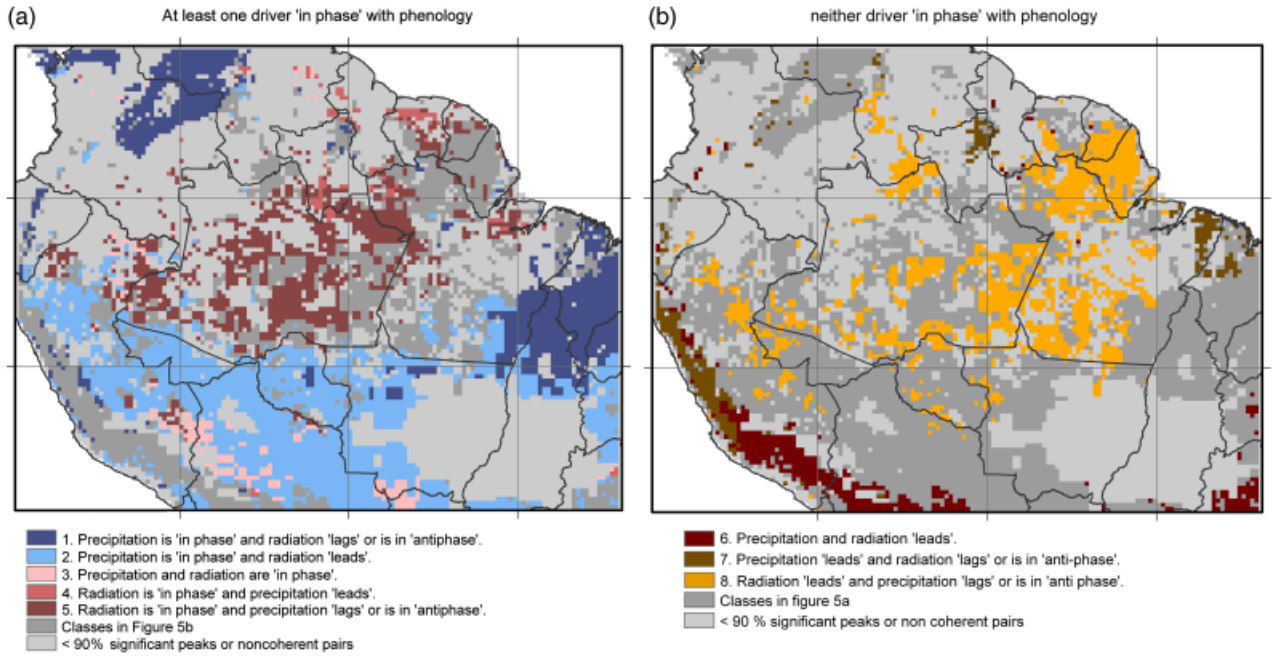

Fig. 5 Major areas of the combined radiation and precipitation phase relationships with phenology, (a) Areas where phenology/EVI is 'in phase' with at least one driver, classes 1–5 and (b) areas where phenology/EVI is not 'in phase' with either driver, classes 6–8.

ency (0.97). Precipitation–phenology is 'in phase' because the phase error is within the 1.0-month limit ($+0.45 \pm 0.29$ months). Radiation has high coherency with phenology (0.95) but the phase is statistically indistinguishable from 'in antiphase' ($+5.75 \pm 0.39$ months). In this case, the phenology is probably driven by precipitation, but not radiation.

Location C (Fig. 6c) is situated in savanna. The radiation lags phenology (-2.75 ± 0.40 months) with very high coherency (0.94). Precipitation leads the phenology ($+1.96 \pm 0.63$ months) with a high coherency (0.87). Although there is a strong seasonality in all variables and high coherency between the time series both drivers are out of phase with phenology. Unlike Location A at Location C probably precipitation, but certainly not radiation given its lag, is apparently driving the phenology.

Discussion and conclusions

The relative power of phenology has similar spatial patterns to the seasonal amplitude of LAI in the Amazon basin (Myneni *et al.*, 2007), but where the time series are good we are able to define areas where the phenology seasonality is weakest, not significant or is not detectable. Surrounding the basin to the north and south, the savanna, and to the west, the mountain grasslands have a much higher relative power and coincide with areas where there are marked wet and dry seasons. High seasonal amplitudes of LAI in the Amazon basin, 1.0–1.2 (Myneni *et al.*, 2007), actually represent rather weak signals in the context of the whole Amazon region. The implications of finding that the seasonality of Terra Firme vegetation is weaker than that of savanna regions is that in Terra Firme areas the annual cycle of radiation may not be as dominant as suggested previously (Myneni *et al.*, 2007) and only drive a small change in phenology seasonality, i.e. weak amplitude. Despite the weak seasonality and weak annual cycles, precipitation still has a role to play in the maintenance of Terra Firme phenology cycles because near continuous precipitation maintains constant vegetation growth (and a relatively high EVI value) reducing the seasonal impact of radiation to weak seasonal cycles of phenology.

The results show structured patterns and gradients of phenology relative power [Fig. 2a(i)] which are indicative of underlying localized environmental controls. The controls that could influence the strength in phenology seasonality include, soil type and drainage: topography; geomorphic units; prevailing environmental conditions; and previous disturbance. One or several of these factors combined can influence leaf size (Malhado *et al.*, 2009) and foliar properties (Fyllas *et al.*, 2009) and given that soil characteristics can vary with depth (Quesada *et al.*, 2009) the locations where plants can reach soil moisture (Nepstad *et al.*, 1994; Malhi *et al.*,

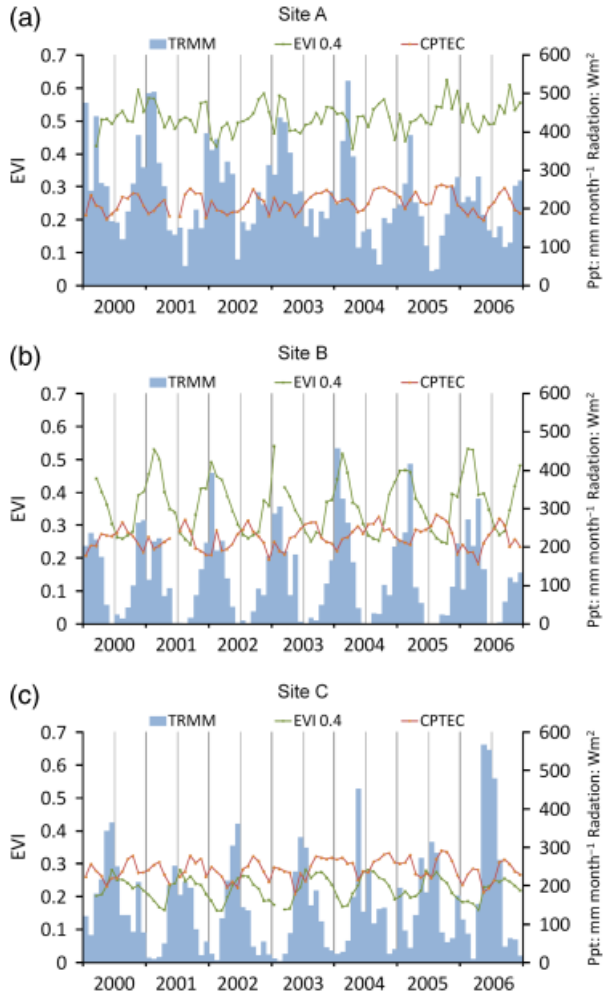

Fig. 6 Enhanced Vegetation Index (EVI), net radiation and precipitation time series between 2000 and 2006 for locations (Fig. 1): (a) A (radiation 'in phase' with phenology/EVI): (b) B (precipitation 'in phase' with phenology/EVI); and (c) C (neither 'in phase' with phenology/EVI). The left hand axis is the EVI, scale 0 to 1.0. The right-hand axis refers to net radiation ($W\,m^2$) and precipitation ($mm\,month^{-1}$). Refer to Table 3 for statistics from the cross-spectral analysis.

1998; da Rocha *et al*., 2004; Huete *et al*., 2006) are difficult to predict. It is also difficult to predict the complete phenology cycle from a single driver since each phenology event could be triggered by different drivers, for example Coronado *et al*. (2009) show regional climate and soil fertility can be related to the floristic composition of Terra Firme forests whereas Chave *et al*. (2010) found that rainfall or soil type does not correlate well with leaf litter fall. To complicate matters, Wright & van Schaik (1994) have also observed that under the same conditions the timing of phenology events can vary between species, within species and on the crowns of individual trees. Furthermore, the strength in seasonality may be influenced by spatial patterns in productivity (e.g., Malhi *et al*., 2004; Aragão *et al*., 2009) and biomass variation (Baker *et al*., 2009) and this may vary in the temporal dimension as vegetation responds to droughts (e.g. Nepstad *et al*., 2007; Phillips *et al*., 2009).

These combined factors have an impact on the detection of the precise timing of phenological events, such as green up, litter fall and leaf abscission at 1×1 km resolution, however, given the localized variation in drivers, the diversity of species and their different phenological behaviour our satellite data can still be used to identify statistically significant annual cycles at this resolution in most of the Terra Firme forest. The phenology cycle of all plant species in a particular pixel will therefore be between two extremes, well synchronized, where species and environmental characteristics are similar, yielding significant power spectral peaks, to poorly synchronized where species assemblages and environmental controls are complex. The latter extreme is probably at least partly responsible for the weakest peaks, nonsignificant peaks and locations with no annual phenology cycle.

We also have to consider that there is a vertical dimension to phenology, and *in situ* observations suggest phenology events may be staggered and tiered between the forest canopy and understory. In the canopy of Terra Firme forest in central Amazonia, Peres (1994) noted distinct seasonal flushing of leaves and Haugaasen & Peres (2005) showed small but significant seasonality in leaf abscission and leaf flushing. In these areas, emergent trees and canopy closure trees can have a tendency to be more deciduous and seasonal than the lower stories which may cause seasonal structural and shadow variations influencing EVI values (Anderson *et al*., 2010, 2011). Since satellites observe from above, the relative amplitude of EVI variations is likely to relate more to phenology events in the upper canopy in cases of high LAI. The relative power is reduced in comparison to the savanna regions because green cover is maintained in the lower strata of the forest. Considering all these aspects, the relative power of the phenology is likely to be a combined function and observation of three factors: (i) how well the phenology is synchronized between all the vegetation inside a single pixel; (ii) the proportion of deciduous vegetation in the pixel and (iii) in dense forest an indication of events in the upper canopy.

There is a scale limitation to our results, we cannot see deciduousness in 30×30 m pixels (Bohlman, 2010) within 1×1 km pixels, and for this reason we may not always agree with *in situ* observations, e.g. precipitation drives young leaf maxima (Peres, 1994) where we predict that precipitation lags phenology. However, our results convey a substantial amount of information

Table 3 Values of relative power, coherency, and phase at the annual scale for locations A (radiation in phase with phenology/EVI), B (precipitation in phase with phenology/EVI) and C (neither radiation nor precipitation in phase with phenology/EVI)

Metric	Location variables	A: Terra Firme forest 04° 31′ 21.23″ S 66° 34′ 39.56″ W	B: Savanna 07° 34′ 44.99″ S 46° 12′ 55.10″ W	C: Savanna 03° 35′ 43.46″ N 60° 33′ 15.68″ W
Power	Phenology	0.11	0.24	0.20
	Radiation	0.09	0.07	0.10
	Precipitation	0.20	0.24	0.15
Coherency	Radiation–phenology	0.87	0.95	0.94
	Precipitation-Phenology	0.79	0.97	0.87
Phase in months (± 95% CI)	Radiation–phenology	0.13 (± 0.63)	−5.75 (± 0.39)	−2.75 (± 0.40)
	Precipitation–phenology	−4.13 (± 0.88)	0.45 (± 0.29)	1.96 (± 0.63)

Location of A, B and C in the Amazon basin is shown in Fig. 1.
Time series for A, B and C are shown in Fig. 6.
EVI, Enhanced Vegetation Index; 95% CI, 95% confidence interval.

at the continental scale beyond the footprint of *in situ* localized investigations.

Examining the patterns of the phase relationships with vegetation, we generally agree that many areas of the Amazon are radiation driven in Terra Firme forest (Nemani *et al*., 2003; Huete *et al*., 2006; Myneni *et al*., 2007). These findings are consistent with many areas of correlation coefficient ~0.4 and above between radiation and LAI calculations by Myneni *et al*. (2007). The time series location A illustrates how these phase differences work on an annual basis: on average while radiation is 'in phase' with EVI, precipitation lags EVI.

Outside the area studied by Myneni *et al*. (2007), are the savanna regions where the 'precipitation in phase with phenology' category dominates, confirming that precipitation is the main driver of the major savanna regions (Sarmiento & Monasterio, 1975). Not surprisingly, the 'precipitation in phase with phenology' scenario is found over large areas in the south and south-east and along the eastern Andes mountain range where the vegetation is dominated by savanna, shrub or grassland (e.g. location B). On the Nemani *et al*. (2003) map most of northern South America is being dominated by radiation with an increasing importance of water around the limits of the study area. By comparison, our phase diagrams show that a smaller region is likely to be dominated by 'radiation in phase with phenology' and there are greater areas of 'precipitation in phase with phenology' surrounding the Amazon basin. We also discover an exception to the radiation phenology–driver relationship. The south-western margins of the Terra Firme forests appear to be precipitation driven and coincide with an area classed as seasonal forest (Saatchi *et al*., 2007) which is a good indication that our results are not an artefact of the vegetation classes we used. Radiation and LAI correlations by Myneni *et al*. (2007) tend to be high but concur with zero correlation coefficients in the same vicinity of the Amazon basin. Furthermore, observed reduction in net primary productivity due to prolonged drought supports this area as water limited (Zhao & Running, 2010).

The in-phase category has established areas where radiation and/or precipitation act as the phenology driver with the vegetation responses occurring within a month. Figure 3h shows that where the drivers are in antiphase with each other in a belt running from north-west to south-west in the north of the study area a single driver explanation for phenology is strongest. Additionally, precipitation drives phenology in the highland region near Brasilia in the south-east of the area where there are no significant annual cycles in radiation. Overall, our average conditions show that most of the Terra Firme forest area is dominated by radiation in-phase or leading phenology (e.g. Fig. 5, classes 3–6, 8). In the savanna and grasslands region, phenology is typically in phase with precipitation. Here radiation can coexist as a driver where it is in antiphase. In savannas, radiation in antiphase with phenology (e.g. to the south-east of class 8 areas in Fig. 5b) could be considered a coexisting driver as this might suppress grassland growth. High light levels could be associated with drying of shallow roots and suppression of photosynthesis (rather than more light encouraging photosynthesis in well-watered Terra Firme forest e.g. at location A). A simple correlation (cf. Nemani *et al*., 2003) would not necessarily have identified the various phase relationships specifically at the annual scale, but our cross-spectral analysis has captured these differences.

There are also areas where neither driver is in phase with EVI such as classes 6–8 in Fig. 5b, Location C demonstrates this pattern. It is more likely that soil moisture, deep roots (Nepstad *et al*., 1994; Malhi *et al*., 1998; Saleska *et al*., 2003; da Rocha *et al*., 2004; Huete *et al*., 2006) and physiological behaviour of plant species (Wright & van Schaik, 1994) are driving the phenology

cycles in those areas. Many of these 'out of phase' regions also coincide with wetland, seasonally flooded regions and can be linked to the rise and fall of rivers. Synchronized leaf shedding and flushing during high water in tune with seasonal cycles and patterns of inundation in both Várzea and Igapó flooded forests were observed by Haugaasen & Peres (2005). Out of phase areas also coincide with agricultural areas where the original vegetation has been replaced with annual crops or pasture and are under the influence of farm management cycles. This may be a deficiency of EVI in agricultural areas where Ferreira *et al*. (2010) found that NDVI has a better seasonal response than EVI. This is difficult to verify from our results without more detailed research.

The maps presented here are being taken forward as a basis to enhance vegetation models with increasingly sophisticated depictions of ecosystem processes. Firstly at the pixel level, synchronicity of phenology may help determine locations that would respond in the same way to climate change (e.g. the Amazon dieback, Cox *et al*., 2004). The amount of deciduousness and behaviour in the upper canopy may assist in estimating cohorts of plants and different age classes within the same biome (e.g. the Ecosystem Demography model, Moorcroft et al., 2001). Secondly, the driver zones can be used to help land surface models in tropical regions to force the timing of phenology events to driving forces (Bradley *et al*., 2009) and investigate what may happen in wet or dry years (e.g. greening up, Saleska *et al*., 2007; Samanta *et al*., 2010, 2011).

The cross-spectral analysis can shed light on the coincidence of seasonal cycles using a relatively short time series. We have confidence in these results as they generally agree with existing research that links vegetation activity with radiation and precipitation. We have summarized where, when and what sequence radiation and precipitation interact with phenology cycles providing a benchmark for modellers to improve their representation of phenology. On condition that these data sets are available, this method can be transferred to other regions, or with sufficient computing power, globally.

Acknowledgements

Support for A. V. Bradley and F. F. Gerard came from the NERC QUEST initiative, N. Barbier, a European MC IEF FP7 Grant and G. P. Weedon by the Joint DECC and Defra Integrated Climate Programme, DECC/Defra GA01101.

References

Aragão LEOC, Malhi Y, Barbier N, Lima A, Shimabukuro Y, Anderson L, Saatchi S (2008) Interactions between rainfall, deforestation and fires during recent years in the Brazilian Amazon. *Philosophical Transactions of the Royal Society B*, **363**, 1779–1785.

Aragão LEOC, Malhi Y, Metcalfe DB *et al*. (2009) Above- and below-ground net primary productivity across ten Amazonian forests on contrasting soils. *Biogeosciences*, **6**, 2759–2778.

Anderson LO, Aragão LEOC, Shimabukuro Y, Almeida S, Huete A (2011) Use of fraction images for monitoring intra-annual phenology of different vegetation physiognomies in Amazonia. *International Journal of Remote Sensing*, **32**, 387–408.

Anderson LO, Malhi Y, Aragão LEOC, Ladle R, Arai E, Barbier N, Phillips O (2010) Remote sensing detection of droughts in Amazonian forest canopies. *New Phytologist*, **187**, 733–750.

Asner GP, Nepstad D, Cardinot G, Ray D (2004) Drought stress and carbon uptake in an Amazon forest measured with spaceborne imaging spectroscopy. *Proceedings of the National Academy of Sciences*, **101**, 6039–6044.

Baker TR, Phillips OL, Laurence WF *et al*. (2009) Do species traits determine patterns of wood production in Amazonian forests? *Biogeosciences*, **6**, 297–307.

Barbier N, Couteron P, Proisy C, Malhi Y, Gastellu-Etchegorry J-P (2010) The variation of apparent crown size and canopy heterogeneity across lowland Amazonian forests. *Global Ecology and Biogeography*, **19**, 72–84.

Best M (2005) *JULES Technical Documentation*. Meteorological Office, Joint Centre for Hydrometeorological Research, Wallingford, UK.

Bloomfield P (1976) *Fourier analysis of time series: an introduction. Wiley Series in Probability and Mathematical Statistics*. Wiley, New York, 272pp.

Bohlman SA (2010) Landscape patterns and environmental controls of deciduousness in forests of central Panama. *Global Ecology and Biogeography*, **19**, 376–358.

Bradley A, Gerard F, Barbier N *et al*. (2009) Template phenology for vegetation models. *Geoscience and Remote Sensing Symposium, IEEE International*, IGARSS 2009, doi: 10.1109/IGARSS.2009.5417570.

Bradley AV, Millington AC (2006) Spatial and temporal scale issues in determining biomass burning regimes in Bolivia and Peru. *International Journal of Remote Sensing*, **27**, 2221–2253.

Bradley BA, Jacob RW, Hermance JF, Mustard JF (2007) A curve fitting procedure to derive inter-annual phenologies from time series of noisy satellite NDVI data. *Remote Sensing of Environment*, **106**, 137–145.

Bradley BA, Mustard JF (2005) Identifying land cover variability distinct from land cover change: cheatgrass in the Great Basin. *Remote Sensing of Environment*, **94**, 204–213.

Brando PM, Goetz SJ, Baccini A, Nepstad DC, Beck PSA, Christman MC (2010) Seasonal and interannual variability of climate and vegetation indices across the Amazon. *Proceedings of the National Academy of Sciences*, **107**, 14685–14690.

Ceballos JC, Bottino MJ, de Souza JM (2004) A simplified physical model for assessing solar radiation over Brazil using GOES 8 visible imagery. *Journal of Geophysical Research*, **109**, D02211, doi: 10.1029/2003JD003531.

Chave J, Navarrete D, Almeida S *et al*. (2010) Regional and seasonal patterns of litterfall in tropical South America. *Biogeosciences*, **7**, 43–55.

Coronado ENH, Baker TR, Phillips OL *et al*. (2009) Multi-scale comparisons of tree composition in Amazonian terra firme forests. *Biogeosciences*, **6**, 2719–2731.

Cox PM, Betts RA, Collins M, Harris PP, Huntingford C, Jones CD (2004) Amazonian forest dieback under climate-carbon cycle projections for the 21st century. *Theoretical and Applied Climatology*, **78**, 137–156.

Cox PM, Betts RA, Jones CD, Spall SA, Totterdell IJ (2000) Acceleration of global warming due to carbon-cycle feedbacks in a coupled climate model. *Nature*, **408**, 184–187.

da Rocha HR, Goulden ML, Miller SD, Menton MC, Pinto LDVO, de Freitas HC, Figueira AMES (2004) Seasonality of water and heat fluxes over a tropical forest in eastern Amazonia. *Ecological Applications*, **14**, S22–S32.

Diggle P (1989) *Time Series: A Biometrical Introduction*. Clarendon Press, Oxford.

Eva HD, Belward AS, De Miranda EE *et al*. (2004) A land cover map of South America. *Global Change Biology*, **10**, 731–744.

Ferreira LG, Huete AR (2004) Assessing the seasonal dynamics of the Brazilian Cerrado vegetation through the use of spectral vegetation indices. *International Journal of Remote Sensing*, **25**, 1837–1860.

Ferreira LG, Yoshioka H, Huete A, Sano EE (2003) Seasonal landscape and spectral vegetation index dynamics in the Brazilian Cerrado: an analysis within the Large-Scale Biosphere–Atmosphere Experiment in Amazonia (LBA). *Remote Sensing of Environment*, **87**, 534–550.

Ferreira NC, Ferreira LG, Huete AR (2010) Assessing the response of the MODIS vegetation indices to landscape disturbance in the forested areas of the legal Brazilian Amazon. *International Journal of Remote Sensing*, **31**, 745–759.

Fyllas NM, Patiño S, Baker TR *et al*. (2009) Basin-wide variations in foliar properties of Amazon forest: phylogeny, soils and climate. *Biogeosciences*, **6**, 2677–2708.

Haugaasen T, Peres CA (2005) Tree phenology in adjacent Amazonian flooded and unflooded forests. *Biotropica*, **37**, 620–630.

Hermance JF (2007) Stabilising high-order, non-classical harmonic analysis of NDVI data for average annual models by damping model roughness. *International Journal of Remote Sensing*, **28**, 2801–2819.

Hermance JF, Jacob RW, Bradley BA, Mustard JF (2007) Extracting phenological signals from multiyear AVHRR NDVI time series: framework for applying high order annual splines with roughness damping. *IEEE Transactions on Geoscience and Remote Sensing*, **45**, 3264–3276.

Houghton RA, Lawrence KT, Hackler JL, Brown S (2001) The spatial distribution of forest biomass in the Brazilian Amazon: a comparison of estimates. *Global Change Biology*, **7**, 731–746.

Huete A, Didan K, Miura T, Rodriguez EP, Gao X, Ferreira LG (2002) Overview of radiometric and biophysical performance of the MODIS vegetation indices. *Remote Sensing of Environment*, **83**, 195–213.

Huete A, Justice C, van Leeuwen W (1999) *MODIS Vegetation Index (MOD13)*. Algorithm Theoretical Basis Document, 129pp. Available at: http://modis.gsfc.nasa.gov/data/atbd/atbd_mod13.pdf (accessed 20 January 2011).

Huete AR, Didan K, Shimabukuro YE *et al*. (2006) Amazon rainforests green-up with sunlight in the dry season. *Geophysical Research Letters*, **33**, L06405, doi:10.1029/2005GL025583.

Jakubauskas ME, Legates DR, Kastens JH (2001) Harmonic analysis of time-series AVHRR NDVI data. *Photogrammetric Engineering and Remote Sensing*, **67**, 461–470.

Jakubauskas ME, Peterson DL, Kastens JH, Legates DR (2002) Time series remote sensing of landscape-vegetation interactions in the southern Great Plains. *Photogrammetric Engineering and Remote Sensing*, **68**, 1021–1030.

Jenkins GM, Watts D (1968) *Spectral Analysis and its Applications*. Holden-Day, San Francisco, London, 541pp.

Kummerow C, Barnes W, Kozu T, Shiue J, Simpson J (1998) The Tropical Rainfall Measuring Mission (TRMM) sensor package. *Journal of Atmospheric and Ocean Technology*, **15**, 809–817.

Lunetta RS, Knight JF, Ediriwickrema J, Lyon JG, Worthy LD (2006) Land-cover change detection using multi-temporal MODIS NDVI data. *Remote Sensing of Environment*, **105**, 142–154.

Malhado ACM, Malhi Y, Whittaker RJ *et al*. (2009) Spatial trends in leaf size of Amazonian rainforest trees. *Biogeosciences*, **6**, 1563–1576.

Malhi Y, Baker TR, Phillips OL *et al*. (2004) The above-ground coarse wood productivity of 104 Neotropical forest plots. *Global Change Biology*, **10**, 563–591.

Malhi Y, Nobre AD, Grace J, Kruijt B, Pereira MGP, Culf A, Scott S (1998) Carbon dioxide transfer over a Central Amazonian rain forest. *Journal of Geophysical Research*, **103**, 31593–31612.

Mann ME, Lees JM (1996) Robust estimation of background noise and signal detection in climatic time series. *Climatic Change*, **33**, 409–445.

Miranda AC, Miranda HS, Lloyd J *et al*. (1997) Fluxes of carbon, water and energy over Brazilian cerrado: an analysis using eddy covariance and stable isotopes. *Plant, Cell and Environment*, **20**, 315–328.

Monasterio M, Sarmiento G (1976) Phenological strategies of plant species in the tropical savannas and the semi-deciduous forest of the Venezuelan Llanos. *Journal of Biogeography*, **3**, 325–356.

MRT (2008) *MODIS reprojection tool user's guide*. Available at http://lpdaac.usgs.gov/landdaac/tools/modis/info/MRT_Users_Manual.pdf (accessed on April 19, 2008).

Moody A, Johnson DM (2001) Land-surface phenologies from AVHRR using the discrete Fourier transform. *Remote Sensing of Environment*, **75**, 305–323.

Moorcroft PR, Hurtt GC, Pacala SW (2001) A method for scaling vegetation dynamics: the Ecosystem Demography model (ED). *Ecological Monographs*, **71**, 557–585.

Myneni RB, Yang WZ, Nemani RR *et al*. (2007) Large seasonal swings in leaf area of Amazon rainforests. *Proceedings of the National Academy of Sciences*, **104**, 4820–4823.

NASA (2006) *Tropical rainfall measuring mission (TRMM) and other data*. Product 3B-43. Available at http//trmm.gsfc.nasa.gov/3b43.html (accessed on January 20, 2010).

Nepstad DC, de Carvalho CR, Davidson EA *et al*. (1994) The role of deep roots in the hydrological and carbon cycles of Amazonian forests and pastures. *Nature*, **372**, 666–669.

Nepstad DC, Tohver IM, Ray D, Moutinho P, Cardinot G (2007) Mortality of large trees and lianas following experimental drought in an Amazon forest. *Ecology*, **88**, 2259–2269.

Nemani RR, Keeling CD, Hashimoto H *et al*. (2003) Climate-driven increases in global terrestrial net primary production from 1982 to 1999. *Science*, **300**, 1560–1563.

Oliveira LMT, França GB, Nicácio RM, Antunes MAH, Costa TCC, Torres AR, França JRA (2010) A study of the El Niño-Southern Oscillation influence on vegetation indices in Brazil using time series analysis from 1995 to 1999. *International Journal of Remote Sensing*, **31**, 423–437.

Olson DM, Dinerstein E, Wikramanayake ED *et al*. (2001) Terrestrial ecoregions of the world: a new map of life on Earth. *BioScience*, **51**, 933–938.

Peres CA (1994) Primate responses to phenological changes in Amazonian Terra Firme forest. *Biotropica*, **26**, 98–112.

Phillips OL, Aragão LEOC, Lewis SL *et al*. (2009) Drought sensitivity of the Amazon rainforest. *Science*, **323**, 1344–1347.

Priestley MB (1981) *Spectral Analysis and Time Series*, 2 vols. Academic Press, London, 890pp.

Quesada CA, Lloyd J, Schwarz M *et al*. (2009) Regional and large-scale patterns in Amazon forest structure and function are mediated by variations in soil physical and chemical properties. *Biogeosciences Discussions*, **6**, 3993–4057.

Reich PB, Borchert R (1984) Water-stress and tree phenology in a tropical dry forest in the lowlands of Costa-Rica. *Journal of Ecology*, **72**, 61–74.

Saatchi SS, Houghton RA, Dos Santos Alvalá RC, Soares JV, Yu Y (2007) Distribution of above ground live biomass in the Amazon basin. *Global Change Biology*, **13**, 816–837.

Saleska SR, Didan K, Huete AR, da Rocha HR (2007) Amazon forests green-up during 2005 drought. *Science*, **318**, 612–612.

Saleska SR, Miller SD, Matross DM *et al*. (2003) Carbon in Amazon forests: unexpected seasonal fluxes and disturbance-induced losses. *Science*, **302**, 1554–1557.

Salazar LF, Nobre CA, Oyama MD (2007) Climate change consequences on the biome distribution in tropical South America. *Geophysical Research Letters*, **34**, L09708, doi:10.1029/2007GL029695.

Samanta A, Ganguly S, Hashimoto H *et al*. (2010) Amazon forests did not green-up during the 2005 drought. *Geophysical Research Letters*, **37**, L05401, doi:10.1029/2009GL042154.

Samanta A, Ganguly S, Myneni RB (2011) MODIS enhanced vegetation index data do not show greening of Amazon forests during the 2005 drought. *New Phytologist*, **189**, 11–15.

Sarmiento G, Monasterio M (1975) A critical consideration of the environmental conditions associated with the occurrence of savanna ecosystems in tropical America. In: *Tropical Ecological Systems* (eds Golley FB, Medina E), pp. 223–250. Springer-Verlag, New York.

Silva Dias MAF, Rutledge S, Kabat P *et al*. (2002) Cloud and rain processes in biosphere–atmosphere interaction context in the Amazon region. *Journal of Geophysical Research*, **107**, 8072, doi: 10.1029/2001JD000335.

Valenti MW, Cianciaruso MV, Batalha MA (2008) Seasonality of litterfall and leaf decomposition in a cerrado site. *Brazilian Journal of Biology*, **68**, 459–465.

Vourlitis GL, Priante-Filho N, Hayashi MMS, Nogueira JD, Caseiro FT, Campelo JH (2001) Seasonal variations in the net ecosystem CO_2 exchange of a mature Amazonian transitional tropical forest (cerradão). *Functional Ecology*, **15**, 388–395.

Vourlitis GL, Priante-Filho N, Hayashi MMS, Nogueira JD, Raiter F, Hoegel W, Campelo JH (2004) Effects of meteorological variations on the CO_2 exchange of a Brazilian transitional tropical forest. *Ecological Applications*, **14**, 89–100.

Wagenseil H, Samimi C (2006) Assessing spatio-temporal variations in plant phenology using Fourier analysis on NDVI time series: results from a dry savannah environment in Namibia. *International Journal of Remote Sensing*, **27**, 3455–3471.

Weedon GP (2003) *Time-Series Analysis and Cyclostratigraphy. Examining Stratigraphic Records of Environmental Cycles*. Cambridge University Press, Cambridge, 259pp.

Werth D, Avissar R (2002) The local and global effects of Amazon deforestation. *Journal of Geophysical Research*, **107**, 8087, doi: 10.1029/2001JD000717.

Wielicki BA, Wong TM, Allan RP *et al*. (2002) Evidence for large decadal variability in the tropical mean radiative energy budget. *Science*, **295**, 841–844.

Wright SJ, van Schaik CP (1994) Light and the phenology of trees. *The American Naturalist*, **143**, 192–199.

Zhao M, Running SW (2010) Drought-induced reduction in global terrestrial net primary production from 2000 through 2009. *Science*, **329**, 940–943.